Impact of the Antenna on the Sub-Terahertz Indoor Channel Characteristics: An Experimental Approach

Priyangshu Sen*, Sherif Badran †, Vitaly Petrov†, Arjun Singh*, and Josep M. Jornet†

*Department of Engineering, SUNY Polytechnic Institute, Utica, NY, USA

†Department of Electrical and Computer Engineering, Northeastern University, Boston, MA, USA

Abstract—Terahertz-band (100 GHz-10 THz) communication is a promising radio technology envisioned to enable ultrahigh data rate, reliable and low-latency wireless connectivity in next-generation wireless systems. However, the low transmission power of THz transmitters, the need for high gain directional antennas, and the complex interaction of THz radiation with common objects along the propagation path make crucial the understanding of the THz channel. In this paper, we conduct an extensive channel measurement campaign in an indoor setting (i.e., a conference room) through a channel sounder with 0.1 ns time resolution and 20 GHz bandwidth at 140 GHz. Particularly, the impact of different antenna directivities (and, thus, beam widths) on the channel characteristics is extensively studied. The experimentally obtained dataset is processed to develop the path loss model and, subsequently, derive key channel metrics such as the path loss exponent, delay spread, and K-factor. The results highlight the multi-faceted impact of the antenna gain on the channel and, by extension, the wireless system and, thus, show that an antenna-agnostic channel model cannot capture the propagation characteristics of the THz channel.

Index Terms—Terahertz communications, ultrabroadband channel sounding, channel modeling, indoor channels.

I. Introduction

Sub-terahertz (100 GHz–300 GHz) communications have been identified among the prospective radio technologies for wireless connectivity in sixth-generation (6G) wireless systems and beyond. The latest predictions account for the rapid development of sub-THz hardware over the recent decade [1], [2] and list sub-THz radio among the technologies for 6G sub-THz wireless backhaul [3], 6G sub-THz network sensing [4], and 6G sub-THz indoor wireless access [5]. Harnessing a new frequency range for an existing scenario typically starts with delivering an understanding of the new wireless channel itself. Here, sub-THz indoor links are not an exception with dozens of measurement and modeling results reported to date [6]. For instance, the impact of frequency has been explored in [7] among others. The impact of distance has been studied in depth in [8], and multiple other works. The impact of the environment itself has been explored in multiple studies, including but not limited to [9]. Admitting the importance and usefulness of prior studies, in this paper, we primarily focus on the implications of the sub-THz antenna used for the measurements (and for future sub-THz communication systems). Moreover, we specifically advocate for the following important conclusion with our results: For 6G and beyond sub-THz radios, there is a clear need to carefully revisit the approach of how a channel model is built.

Specifically, a notable fraction of existing 5G-grade models [10] are built roughly following three steps. First, the measurement campaign is conducted. Then, the measured values get post-processed to compensate for the effect of the used antennas. Finally, there is a method to tailor the delivered model to any desired antenna characteristics. The existing "antenna-agnostic" models are very convenient for microwave and even low mmWave systems (e.g., most common 5G New Radio Frequency Range 2 frequencies 24 GHz - 30 GHz). However, extrapolating the same approach to sub-THz bands leads to severe issues during both Stage 2 and Stage 3 above, as the antenna impact cannot be easily decoupled from the channel impact anymore. Specifically, as further reported in the paper, some large-scale antennas for sub-THz bands have non-negligible near-field zones of several meters or even tens of meters with complex relationships with the observed channel metrics [11]. The occurrence of the waveguide tunneling effect in indoor settings can also have a non-negligible impact [12].

There have been attempts to characterize the impact of antenna directivity with ray-tracing modeling [13]. However, those techniques have limited applicability in the near field. The "near-field-to-far-field transition" when changing the antenna configuration leads to a notable deviation in the expected and observed results even in simple line-of-sight (LoS) conditions. Further, sub-THz antennas of different directivity nonlinearly affect the multi-path nature of the received signal, consequently impacting e.g., the delay spread and K-factor in complex ways. Hence, applying the 5G-grade solutions to decouple the antenna-centric effects from channel-centric effects in the measured data, results in notable errors introduced. To the best of the authors' knowledge, this is one of the first measurement-based studies on antenna-centric effects in sub-THz indoor channels, highlighting and quantifying this important mismatch, as well as suggesting possible ways to partially address the issue.

The major contributions of this paper are thus as follows:

- We deliver new measurement results in an indoor configuration with different sub-THz antennas that can be used as reference points for further modeling and performance evaluation efforts in this research area.
- We further present simple parametric models to characterize the major trends, dependencies, and trade-offs in the observed measurement results.

The rest of the paper is organized as follows. Sec. II introduces our measurement setup used for our sub-THz indoor channel sounding. Then, Sec. III summarizes the major measurement and modeling results, as well as the key observations highlighting the importance and difficulty of incorporating the antenna characteristics into the existing models. Finally, Sec. IV concludes the paper and outlines possible further steps in this research direction.

II. MEASUREMENT SETUP

Herein, we first describe the channel sounder system and then the indoor setup for our measurement campaign.

A. NU Channel Sounder

The channel sounder at Northeastern University (NU), or NU Channel Sounder, is a tailored spread spectrum-based sliding correlator type channel sounder [14]. It can capture multipath profiles with high resolution and dynamic range.

1) Terahertz Sounder Frontends: The frontend components of the channel sounder are developed through the TeraNova testbed [15], [16]. The transmitter and receiver components, along with the rotatory table, are shown in Fig. 1 (a) and (b), respectively. At the transmitter, we utilize an arbitrary waveform generator (AWG) to generate baseband (BB)/intermediate frequency (IF) spread spectrum-based channel sounding signals with 20 GHz of bandwidth. Multiplier and mixer chains up-convert the BB/IF to the RF frequency starting from a local oscillator (LO). The signal is downconverted by a similar RF system and captured through a digital storage oscilloscope (DSO) for offline processing. A cable is utilized to connect the 10 MHz clock of the LOs at the Tx & Rx for synchronization. An in-home developed absorption material with water-absorbed mat and foam, shown in Fig. 1 (d), is utilized to mitigate the reflection from the metal structure of the receiver itself.

2) Signal Processing Backend: The signal processing backend consists of both transmitter and receiver sections, as shown in Fig. 1(c), and is implemented in MATLAB. We utilize the backend to generate the channel-sounding specific waveform and further process it at the receiver. The transmitted signal frame is made of an 8191-m-sequence header and a 4095chips m-sequence that is repeated 16 times, which is utilized for actual channel measurement. The frame is modulated with binary phase-shift keying (BPSK) and pulse-shaped with a high roll-off factor root-raised cosine filter. The signal is generated through the AWG and up-converted for transmission to the 130-150 GHz band. At the receiver, the captured sampled signal at the DSO is processed, by first utilizing the header to detect the start of a frame. Then, the captured signal is calibrated to eliminate the frequency selective response of the hardware as shown in [14]. The signal-sounding component of the waveform (with repeated 4095 m-sequence) is correlated with a locally generated 4095 m-sequence to extract the channel impulse response. An average of over 16 such repetitions are taken to reduce the noise floor and eliminate false detection. The received power is determined by normalizing with pulse energy and m-seq length (i.e., 4095). Finally, by setting the threshold based on the channel sounder's dynamic range, the peaks, and corresponding delays are measured by the global convergence method. With 20 GHz of RF bandwidth, multipath components with 0.1 ns time resolution can be measured.

B. Sounding Environment and Methodology

The measurement campaign is performed in an indoor conference room of dimension 10m×10m at Northeastern University. The conference room structure, geometrical shape, and placement of the transceiver are shown in Fig. 1 (e),(f) and (g). We have utilized 13 dBm of transmit power with a 15 dBi (30⁰ beamwidth) antenna to transmit the sounding signal at a height of 2 m close to the ceiling. The receiver is kept at the height of 1 m to define the height of the tabletop on the rotatory table in the different places within the room, as shown in Figure 1 (e). The rotatory table is rotated in steps of the beamwidth of the receiving antenna in the azimuth direction to acquire the angular information. We start by ensuring that our transmitter and receiver antennas are perfectly aligned, maintaining LoS. At the receiver, antennas of various gain/beam widths are utilized to collect the received signal. The antennas we have utilized have a gain of 15, 21, 25, and 38 dBi, and beamwidths of 30, 11, 10, and 2°, respectively. All the antennae at the transceiver operate at the D-band frequency range (110-170 GHz).

III. EXPERIMENTAL RESULTS

First, we analyze the path loss model and exponent with various antenna gains. Finally, we moved with the detected multipath profiles and statistically determined channel metrics.

A. Path Loss Model

The path loss models are crucial to estimate power loss over the wireless interface due to multipath interference. The presence of a line-of-sight (LoS) component normally results in representing the path loss through the log-distance model. Here, the path loss PL at a distance d is evaluated through the Friis free space path loss PL $_0$ at $d_0=1\ m$, with the excess loss due to the distance, d, having a path loss exponent (PLE), n. A zero-mean Gaussian distributed random variable, χ , with a standard deviation of σ dB, is introduced to represent the shadow effect. The cumulative path loss PL is given by

$$PL = PL_0 + 10n \log_{10} \left(\frac{d}{d_0}\right) + \chi. \tag{1}$$

We estimate the value of n by mapping the experimental path loss, $L_{\rm PL}$, in dB scale using the maximum likelihood estimation (MLE) method with the model given in (1) for the link budget analysis. Figure 2 presents both the experimental as well as estimated/curve fitted (CF) values of path loss as a function of distance for different antenna gain at the receiver. Figure 3a shows the variation of the path loss exponent with varying antenna gains. The curve fit is given by

$$n(G) = 1.811e^{0.001018G} - 30.15e^{-0.2437G},$$
 (2)

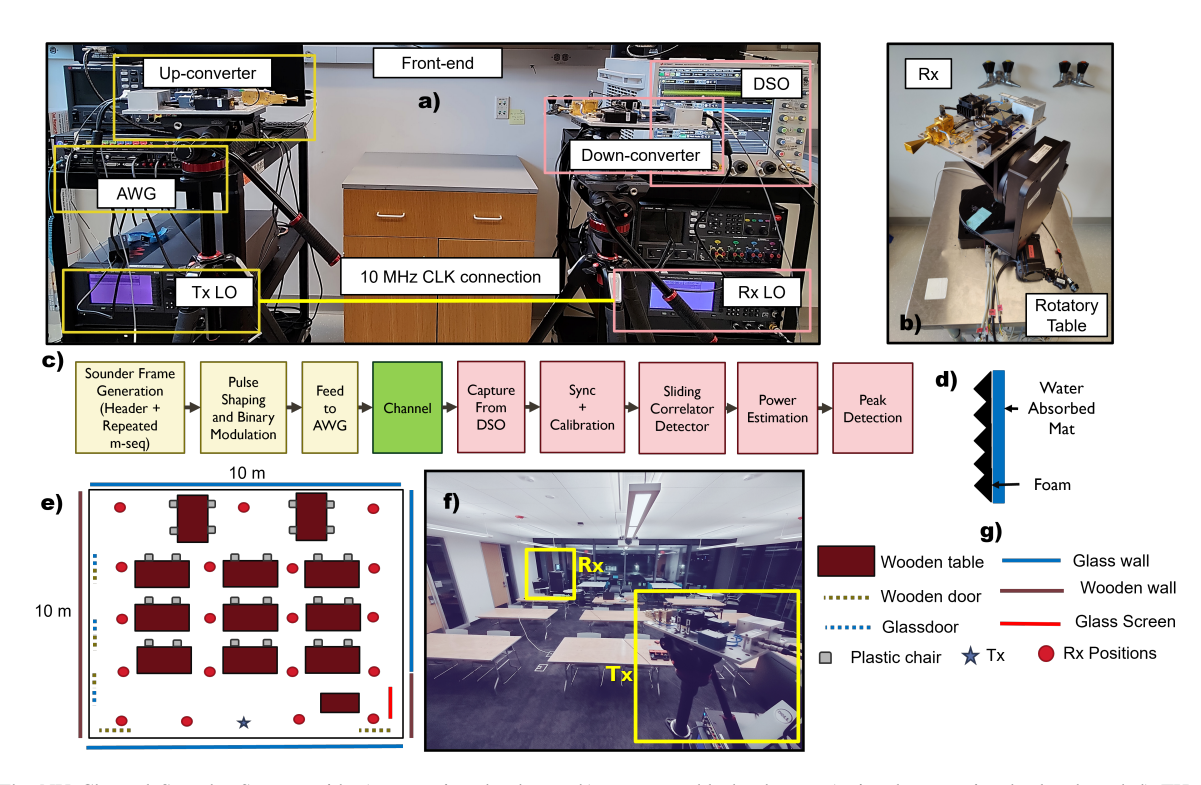


Fig. 1. The NU Channel Sounder System with a) transceiver hardware, b) rotatory table hardware, c) signal processing backend, and d) THz frequency absorption meterial. The conference room details, i.e., the sounding environment, including e) layout, f) picture, and g) legend.

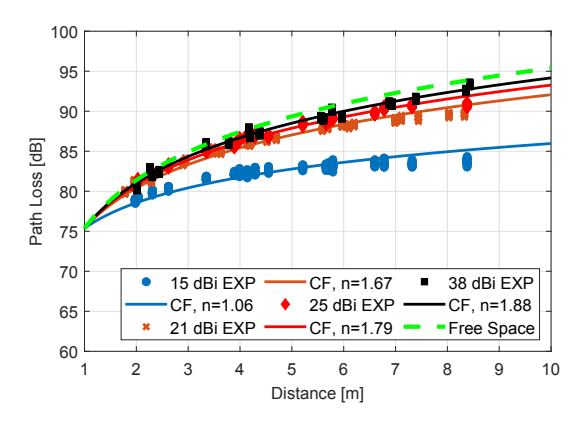


Fig. 2. Path Loss with varying antenna gain (beam width) with experimental (EXP) and curve fitted (CF) value.

where n is the PLE and G is the antenna gain. The value of n < 2 in most cases is caused by the waveguide/tunnel multi-path effect of LoS indoor channel [12]. Further, n increases with an increase in antenna gain (i.e., a decrease in antenna beamwidth). This increase in path loss with antenna gain can not be explained alone by the lowering of the waveguide/tunneling effect as shown in [13] through ray tracing simulation. This can be more clearly understood as the fact that the effective gain of larger gain, and consequently larger sized aperture, is reduced due to the presence of nearfield effects. Specifically, we can estimate the radiated and received beams from these antennas by approximating them as Gaussian beams [17]. We quantify the evaluations for the extreme cases of 15 and 38 dBi antennas, with the other

antennas falling in this range. The 38 dBi antenna is a circular horn-lens antenna (efficiency of 0.45), giving us a Gaussian beam with an aperture $w_{0,38}=59~\mathrm{mm}$ [18]. In contrast, the 15 dBi antenna is an open waveguide, with the effective gain given as [18]:

$$G = 10\log_{10}\left(0.81\frac{4\pi}{\lambda^2}ab\right),\tag{3}$$

where λ is the wavelength, and ab is the product of the width and length of the waveguide. The correction factor of 0.81 comes as $\approx 8/\pi^2$, due to the fact that the electric field across the waveguide is not uniform. We equate this waveguide to a circular aperture with the same efficiency of 0.45, giving the value as $w_{0.15}=4$ mm.

A Gaussian beam generated from an aperture w_0 with an initial electric field E_0 has the field E(z) after propagation in the z-axis given as [17]:

$$E(z) = E_0 \frac{w_0}{w(z)} e^{\left(\frac{-r^2}{w(z)^2} e^{\left(-j(kz + k \frac{r^2}{2R(z)} + \phi(z))\right)}\right)},$$
 (4)

where
$$w(z) = w_0 \sqrt{1 + \left(\frac{z}{z_R}\right)^2}$$
, $R(z) = \frac{z^2 + z_R^2}{z}$,

where w(z) is the beam waist after propagating a distance z, and R(z) is the radius of curvature, with $\phi(z) = \arctan z/z_R$ describing the Gouy phase. $z_R = \pi w_0^2/\lambda$ is the Rayleigh range. The received power $P_{\rm rx}$ from a receiver with an aperture of size $w_{\rm rx}$ at a link distance z is found as:

$$P_{\rm rx} = \int_{-w_{\rm rx}}^{w_{\rm rx}} E(z)^2 \, dr,\tag{5}$$

where E(z) is the electric field from (4). The phase component $-k\frac{r^2}{2R(z)}$, where k is the wavenumber, varies across the cross-sectional aperture $w_{\rm rx}$, and thus the electric field does not add up in phase. We present the beam profile emanating from the 15 dBi transmitter in Fig. 4. The cross-sectional cut is at z=1 m, similar to how PL₀ is set in (1). It can be seen that the beam intercepted by a smaller receiver will have a uniform phase profile, whereas the larger antenna will capture a beam that has multiple variations in the phase, indicating that there will be significant destructive interference, reducing the operational gain, or equivalently, increasing the path loss.

Nonetheless, the deviations of each of the experimentally evaluated curves from each other as well as the conventional free-space path loss model highlight that channel characterization in the THz regime cannot be performed independently of the antenna(s) utilized in the system.

B. Channel Metrics

We characterize and present here the ultra-broadband indoor wireless communication link at 140 GHz in terms of the Rician K-factor, the root mean square (RMS) delay spread (DS), and the angular spread (AS), which are among the crucial metrics for the over the air communication system design. In addition, we have demonstrated the relationship between the metrics and antenna gain/beamwidth.

1) K-factor: The K-factor is a significant metric for LoS link, which provides insight into communication link quality based on the power associated with the LoS and the scatter components. It is defined by the ratio of the power in the LoS path $(P_{\rm LoS})$ and other NLoS paths $(2\ S^2)$, and it thus given by

$$K = \frac{P_{\text{LoS}}}{2S^2}.$$
 (6)

In the dB scale, it is represented by $10\log_{10}(K)$. This metric provides insight into the type of fading a channel could experience. For example, with an increase in the K-factor, the chance of experiencing deep fade reduces and increases the link reliability by reducing the bit error performance. Therefore, the estimation of the K-factor is of practical importance in various wireless scenarios, including channel characterization, adaptive modulation, and localization applications.

The cumulative distribution function (CDF) of the K-factor with different antenna gains within the conference room is shown in Fig. 5 by comparing experimental (EXP) results and curve fitting (CF). The K-factor in the dB scale is approximated by the normal distribution with mean (μ) and standard deviation (σ) for different gains of antenna at the receiver. It is observable that the K-factor mean increases and variance decreases with an increase in antenna gain (i.e., with the decrease in beamwidth). Consequently, wireless THz communications and networks will require innovative adaptive link modulation and coding schemes to adapt to changing channel parameters with changing antenna gain. Figure 3b shows the variation of the K-factor with varying antenna gains. The curve fit is given by:

$$K(G) = 0.03576G^2 - 1.246G + 32.1, (7)$$

where K is the Rician K-factor in dB and G is the antenna gain in dBi.

2) Delay Spread: To analyze the power delay profile of the indoor channel with different antenna gain, the root mean square (RMS) delay spreads (DS), $\tau_{\rm RMS}$, are computed for various receiver positions. The RMS DS is calculated by

$$\tau_{\text{RMS}} = \sqrt{\frac{\sum_{i} (d_{i} - \hat{d})^{2} \ p_{i}^{2}}{\sum_{i} p_{i}^{2}}},$$
 (8)

where d_i and p_i are the delay and received power of propagation path i, respectively, and \hat{d} is the mean delay represented by

$$\hat{d} = \frac{\sum_{i} d_i \ p_i}{\sum_{i} p_i}.\tag{9}$$

The metric statistics is divided into two parts- LoS and NLoS, to have a holistic view considering the sparse nature of the THz channel and the significant difference between the statistics obtained from LoS and NloS components. The CDF of the RMS DS captured for various gain antennas are shown in Fig. 6, which can be approximated as an exponential distribution with mean value β (increase in β produced heavier tail CDF). The value for the DS is notably small (in the range of 2 ns) for both the LoS and NLoS links. Although NLoS components have higher RMS DS and heavier tail distribution compared to LoS (i.e., x3 higher) counterpart. Regardless, the DS is large enough to create ISI, considering the ultra-broadband (20 GHz bandwidth) nature of the signal. Further, the RMS DS increases with the increase in beam width (i.e., a decrease in antenna gain). Therefore, it is crucial to design innovative link adaptation techniques considering the statistical feature of DS based on antenna gain as well as the link condition - LoS or NLoS - when choosing pilot bits. For example, this aspect could be utilized to make an efficient choice for pilot bits to optimize the throughput by considering the 90 percentile point from the CDF curve of RMS DS. Figure 3c shows the variation of the RMS DS with varying antenna gains, for both line-of-sight and non-line-ofsight cases. The trend shows that for both cases, the RMS delay spread decreases with increasing antenna gains (i.e., decreasing antenna beam widths), as the more directional the beam gets, the lesser multipath propagation occurs and thus the lower the delay spread. The curve fit equation is given by,

$$\tau_{\text{RMS}_{\text{LoS}}}(G) = 0.00118G^2 - 0.08012G + 1.583,$$
 (10)

$$\tau_{\text{RMS}_{\text{LoS}}}(G) = 0.001144 G^2 - 0.1964 G + 6.101,$$
 (11)

where $\tau_{\rm RMS}$ is the RMS DS in ns and G is the antenna gain in dBi.

3) Angular Spread: The spatial multipath richness of the wireless channel can be determined by the angular spread (AS), which could be essential to define the link establishment possibility through NLoS. We investigate the RMS angular spread (AS_{RMS}) for the angle of arrival (AOA) in the azimuth direction (θ) to examine the spatial multipath profile at 360-degree angles. For this purpose, we have rotated the receiver

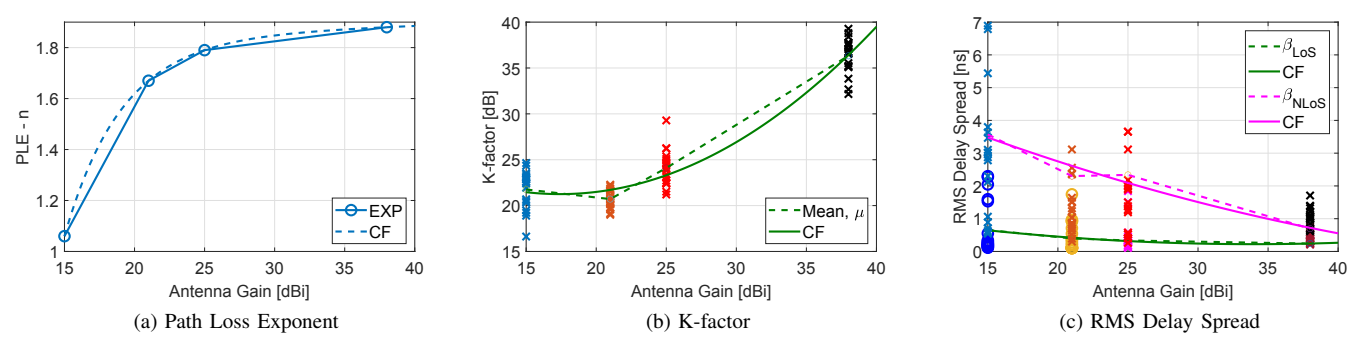


Fig. 3. Experimental and curve-fitted channel parameters with varying antenna gains for the conference room.

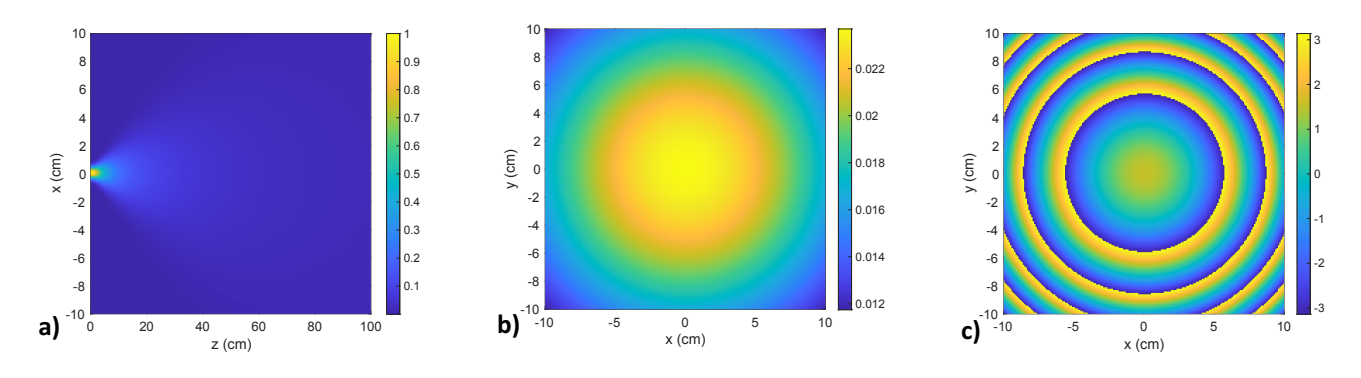


Fig. 4. Beam profile from a 15 dBi antenna: (a) propagation; (b) cross-sectional amplitude; and (c) cross-sectional phase. The cross-sectional cut is at 1 m.

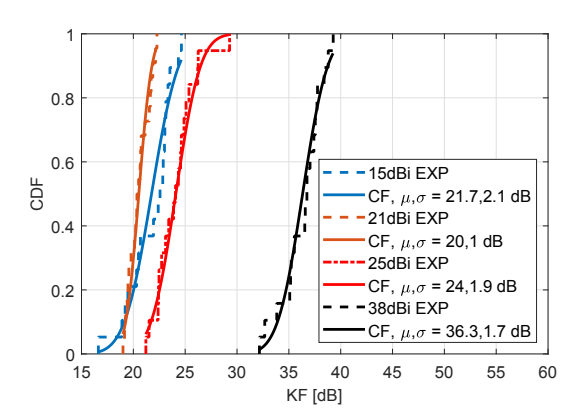


Fig. 5. CDF of K-factor with different antenna gain for EXP result (dotted line) and its CF (solid line) with μ , and σ of log-normal distribution.

in steps of beam width in a horizontal direction. Analytically, it is represented by

$$AS_{RMS} = \sqrt{\frac{\sum_{i} (\theta_i - \hat{\theta})^2 p_i^2}{\sum_{i} p_i^2}},$$
 (12)

where θ_i and p_i are the AOA and received power of propagation path i, respectively, and $\hat{\theta}$ is the mean AOA represented by

$$\hat{\theta} = \frac{\sum_{i} \theta_{i} \ p_{i}}{\sum_{i} p_{i}}.$$
 (13)

The CDF of the AS_{RMS} with different antenna gain obtained from data captured at different positions within the room is shown in Fig. 7. It follows the normal distribution with mean (μ) and standard deviation (σ) . Overall, AS_{RMS} is low due to the sparse nature of NLoS paths, which indicates establishing a reliable communication link over a 360-degree angle is critical in the THz band, and it becomes increasingly challenging as antenna gain increases. It is observed by the fact that σ increases with an increase in antenna gain. Therefore, an extensive and innovative searching algorithm is required to establish a reliable communication link through LoS or significant NLoS components (i.e., link through a highly reflective surface). The AS_{RMS} is highly dependent on the room composition and structure. Therefore, further study of the channel in different indoor scenarios of varying sizes is required to establish a correlation between AS_{RMS}'s statistical parameter and antenna gain.

IV. CONCLUSION

This paper reports channel-sounding measurements for ultra-broadband links in the 130–150 GHz band with various antenna gains. The results show the impact of the antenna directivity & beam width on the channel characteristics beyond a change in gain. Although providing environment-specific insight, these cannot be decoupled from the channel statistics through any single curve fitting or correction term. Thus, the results motivate the development of robust real-time channel

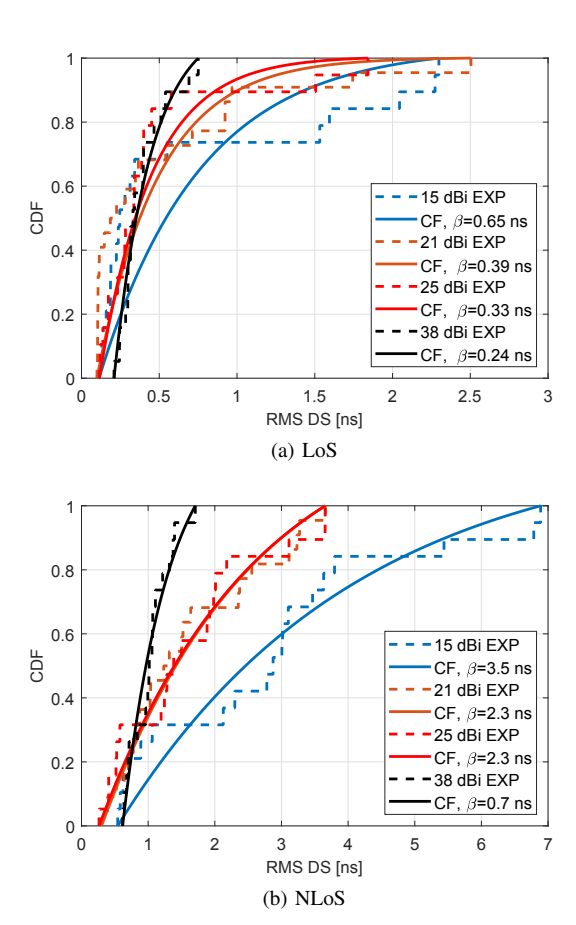


Fig. 6. CDF of RMS DS with different antenna gain for EXP results (dotted line) and its CF (solid line) with β of exponential distribution.

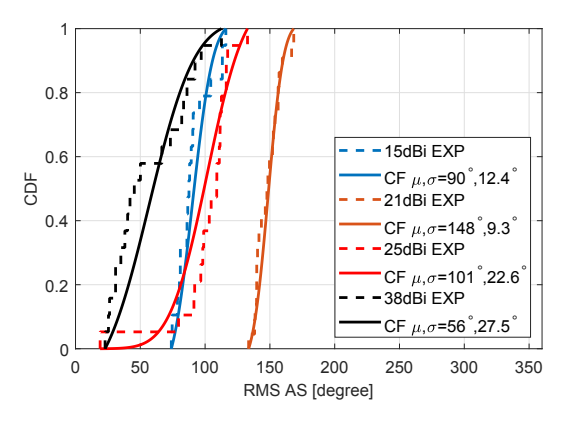


Fig. 7. CDF of RMS AS with different antenna gain for EXP result (dotted line) and corresponding CF (solid line) with μ , and σ of normal distribution.

estimation and link adaption techniques that consider the changes in channel properties when dynamic beams, likely to be generated from a single transmit, receive, or reflect antenna array, are utilized. This also motivated further quantization of the antenna gain in other sub-THz channel studies. Our future work is aimed at increasing the richness of the data set in additional scenarios (indoor, outdoor, aerial), with different structural and geometrical aspects, blockage, and atmospheric conditions at different frequencies above 100 GHz for a broad understanding of the sub-THz channel.

ACKNOWLEDGMENT

This work is funded by the U.S. National Science Foundation under grant CNS-2225590 and the U.S. Air Force Office of Scientific Research under grant FA9550-23-1-0254. The authors would like to thank Jacob Hall, a Northeastern University graduate alumni, for his efforts in developing the control automation and data collection.

REFERENCES

- [1] K. Rasilainen, T. D. Phan, M. Berg, A. Pärssinen, and P. J. Soh, "Hardware aspects of sub-thz antennas and reconfigurable intelligent surfaces for 6G communications," *IEEE Journal on Selected Areas in Communications*, vol. 41, no. 8, pp. 2530–2546, August 2023.
- [2] H. Sarieddeen, M.-S. Alouini, and T. Y. Al-Naffouri, "An overview of signal processing techniques for terahertz communications," *Proceedings* of the IEEE, vol. 109, no. 10, pp. 1628–1665, October 2021.
- [3] Ericsson and Intel, "A concept for evaluating sub-THz communication for future 6G," white paper, 2023.
- [4] Nokia, "Joint design of communication and sensing for Beyond 5G and 6G systems," white paper, April 2021.
- [5] C. Lin and G. Y. Li, "Indoor terahertz communications: How many antenna arrays are needed?" *IEEE Transactions on Wireless Communications*, vol. 14, no. 6, pp. 3097–3107, June 2015.
- [6] D. Serghiou, M. Khalily, T. W. C. Brown, and R. Tafazolli, "Terahertz channel propagation phenomena, measurement techniques and modeling for 6G wireless communication applications: A survey, open challenges and future research directions," *IEEE Communications Surveys & Tutorials*, vol. 24, no. 4, pp. 1957–1996, Q4 2022.
- [7] Y. Xing, T. S. Rappaport, and A. Ghosh, "Millimeter wave and sub-thz indoor radio propagation channel measurements, models, and comparisons in an office environment," *IEEE Communications Letters*, vol. 25, no. 10, pp. 3151–3155, 2021.
- [8] S. Ju, Y. Xing, O. Kanhere, and T. S. Rappaport, "Sub-terahertz channel measurements and characterization in a factory building," in *Proc. of the IEEE ICC*, May 2022, pp. 2882–2887.
- [9] Y. Wang, Y. Li, Y. Chen, Z. Yu, and C. Han, "0.3 THz channel measurement and analysis in an 1-shaped indoor hallway," in *Proc. of* the IEEE ICC, May 2022, pp. 2870–2875.
- [10] 3GPP, "Study on channel model for frequencies from 0.5 to 100 GHz (Release 17)," 3GPP TR 38.901 V17.0.0, March 2022.
- [11] M. Cui, Z. Wu, Y. Lu, X. Wei, and L. Dai, "Near-field MIMO communications for 6G: Fundamentals, challenges, potentials, and future directions," *IEEE Communications Magazine*, vol. 61, no. 1, pp. 40–46, January 2023.
- [12] H. Xu, V. Kukshya, and T. S. Rappaport, "Spatial and temporal characteristics of 60-ghz indoor channels," *IEEE Journal on selected areas in communications*, vol. 20, no. 3, pp. 620–630, 2002.
- [13] S. Priebe, M. Jacob, and T. Kürner, "The impact of antenna directivities on thz indoor channel characteristics," in 2012 6th European Conference on Antennas and Propagation (EUCAP). IEEE, 2012, pp. 478–482.
- [14] P. Sen, J. Hall, M. Polese, V. Petrov, D. Bodet, F. Restuccia, T. Melodia, and J. M. Jornet, "Terahertz communications can work in rain and snow: Impact of adverse weather conditions on channels at 140 GHz," in *Proceedings of the 6th ACM Workshop on Millimeter-Wave and Terahertz Networks and Sensing Systems*, 2022, pp. 13–18.
- [15] P. Sen, V. Ariyarathna, A. Madanayake, and J. M. Jornet, "A versatile experimental testbed for ultrabroadband communication networks above 100 ghz," *Computer Networks*, vol. 193, p. 108092, 2021.
- [16] P. Sen, D. A. Pados, S. N. Batalama, E. Einarsson, J. P. Bird, and J. M. Jornet, "The teranova platform: An integrated testbed for ultra-broadband wireless communications at true terahertz frequencies," *Computer Networks*, vol. 179, p. 107370, 2020. [Online]. Available: https://www.sciencedirect.com/science/article/pii/S1389128620304473
- [17] J. Alda, "Laser and gaussian beam propagation and transformation," Encyclopedia of optical engineering, vol. 999, pp. 1013–1013, 2003.
- [18] C. A. Balanis, Antenna theory: analysis and design. John wiley & sons, 2016.